Proceedings of Global Power and Propulsion Society
ISSN-Nr: 2504-4400
GPPS Xi'an21
18th – 20th October, 2021
www.gpps.global

# GPPS-TC-2021-0356

# FEEDING $H_2$ ADMIXTURES IN A MICRO-GAS TURBINE: A CFD STUDY

**Lorenzo Giuntini**
**University of Pisa**
lorenzo.giuntini@phd.unipi.it
Pisa, Italy

**Chiara Galletti**
**University of Pisa**
chiara.galletti@unipi.it
Pisa, Italy

**Alessandro Parente**
**Université Libre de Bruxelles**
alessandro.parente@ulb.be
Bruxelles, Belgium

## ABSTRACT

A strong integration of renewable energy sources is required to reach decarbonization targets and guarantee sustainable energy production. Green energy carriers as hydrogen can be produced via electrolysis from excess wind and solar power (power-to-gas), allowing chemical energy storage in the form of energy-dense carriers with neutral or even negative carbon balance. Hydrogen and $H_2$ admixtures, hence, play a key role for the energy transition from fossil fuels to renewables. However, hydrogen exhibits much higher reactivity and adiabatic flame temperature than other fuels; this behavior opens technological issues related to flame stabilization and pollutant emissions. Hence, we need to understand the impact of $H_2$ addition on the operation and emissions of existing combustion systems. The objective of the present work is to study the combustion of natural gas (NG) and $H_2$-NG mixtures in a micro-Gas Turbine (mGT) for energy generation, by means of CFD techniques. Different combustion modelling approaches are employed to model properly the combustion regime inside the combustor. CFD provides a detailed analysis of the thermo-fluid dynamics fields, to understand the effect of $H_2$ addition on the mGT behavior.

## INTRODUCTION

In order to decarbonize mobility, industry and power generation, a strong integration of renewable energy sources is required. However, due to the fluctuating nature of these sources, energy storage systems are required to balance out the power grid. One of the most promising solutions for mid-to-long term and high-capacity energy storage is to use the electricity excess from solar and wind power to produce green hydrogen via water electrolysis. In this context, green hydrogen from renewables may be exploited as energy carrier, thus reconverting it into on-demand power and heat. To this purpose, the existing energy supply chain based on the combustion of fossil fuels into Gas Turbine may be exploited to regain energy from hydrogen (Shih et al., 2014). Moreover, green hydrogen may drive the decarbonization of those industries, such as cement, glass and steel making factories, which require high process temperatures achievable only through combustion. However, hydrogen displays combustion properties that are very different from those of other fuels, exhibiting a much higher reactivity and adiabatic flame temperature. For this reason, detailed investigations are required to ensure the safe and efficient operation of existing equipment with $H_2$ admixtures. Computational Fluid Dynamics (CFD) provides a key tool in this perspective, as it allows to gain information on the thermo-fluid dynamic behavior of the combustors. Moreover, CFD allows to investigate the effect of different fuels and operating conditions, as well as to devise geometrical modifications of the burners. The literature acknowledges several works on the use of CFD techniques for the design and optimization of gas turbine combustors fed with hydrogen-enriched fuels. Tomczak et al., 2002. carried out CFD simulations on a diffusion flame gas turbine combustor fed with different $CH_4/H_2$ mixtures. They noticed higher NOx emissions, as the hydrogen content was increased, suggesting water addition or combustion air humidification as possible measures to limit nitrogen oxides formation. Reale et al., 2012, performed RANS simulations to evaluate the influence of low hydrogen concentrations on a commercial micro-Gas Turbine (mGT). Cappelletti et al., 2014, proposed a numerical redesign of the Turbec T100 combustor to operate with 100% $H_2$. In particular they eliminated the premixing region, responsible of flame stability issues, i.e. flashback, making the combustor operates only with diffusion flames. Cameretti

et al., 2020, studied combustion and $NO_x$ formation in a mGT combustor, by feeding both syngas and pure hydrogen. Very recently Pappa et al., 2021, performed LES simulations to compare methane combustion with hydrogen-based fuels combustion in the Turbec T100 combustor, also evaluating the effect of oxidizer humidification.

The present work aims at carrying out CFD simulations to analyse the thermo-chemical and fluid dynamics behaviour of the combustor of a 100 $kW_{el}$ commercial micro-Gas Turbine (mGT). Various combustion models are compared to evaluate how results are affected by the chosen modelling approach. This mGT is designed to operate with natural gas (NG), but off-design operations by adding hydrogen to the fuel mixture are also investigated.

## Combustor description

The Turbec T-100 is a micro-Gas Turbine that operates with combined heat and power generation (Ali et al., 2014), according to the Brayton cycle. In particular, this mGT employs a centrifugal compressor to compress ambient air up to 4.5 bar, at nominal conditions. Subsequently, the air is pre-heated up to 868 K passing through a recuperator, thus it enters the combustion chamber. Here, the reaction between the hot compressed air and fuel takes place, producing hot gases at 1223 K (turbine inlet temperature), which are expanded through a radial turbine, driving the compressor and the generator. Finally, the exhaust gases exiting the turbine at about 923 K are fed to two recuperators to preheat the ingoing ambient air and to produce warm water. The nominal power output is of about 100 $kW_{el}$ and 165 $kW_{th}$, with an electrical efficiency of about 33% and an overall efficiency of 80%. The combustor associated to this mGT employs different air injections and recirculation zones to make the internal temperature uniform, thus controlling $NO_x$ formation. In particular, the main fuel feed is highly diluted and premixed with air, close to the lower flammability limit. For this reason, a non-premixed pilot flame is employed to sustain the combustion. Due to this configuration, the combustion regime can be considered neither purely premixed nor non-premixed. A mid-plane section of the combustor under investigation is shown in Figure 1.

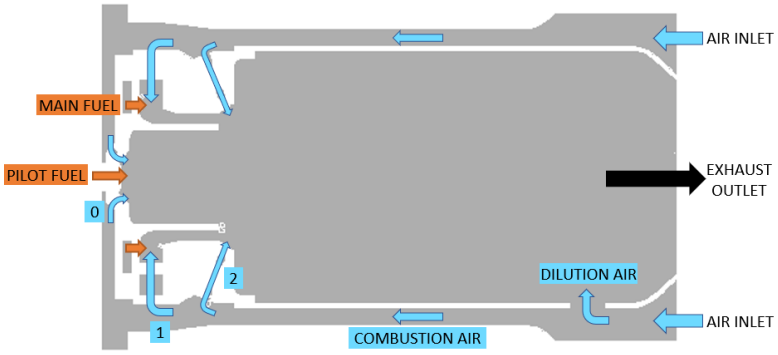


**Figure 1: Mid-plane view of the combustor employed to perform CFD simulations. Some streams are labelled as follows: "0" corresponds to pilot air, "1" to primary air and "2" to secondary air.**

Figure 1 shows how air passes in an external case and enters the combustion chamber through different holes. The main air feed (i.e., AIR INLET in Figure 1) is split into two streams: dilution air and combustion air. Dilution air enters the combustion chamber through 9 dilution holes, which are used to reduce the temperature of the exhaust gases down to 950 °C. On the other hand, combustion air is divided into three streams: pilot air, primary air and secondary air, labelled with "0", "1" and "2" respectively in Figure 1. Pilot air enters the combustion chamber through 12 swirl injectors. In this region, reaction between pilot air and pilot fuel, which is fed through 6 injectors, takes place in non-premixed conditions, producing a diffusion flame. Primary air passes through 15 radial swirling vanes in which it is premixed with an equal number of main fuel streams. As this air/fuel mixture enters the combustion chamber it ignites, due to the heat source provided by the pilot flame, thus resulting in a main premixed flame. Further downstream, secondary air is injected inside the combustion chamber through 30 circumferentially distributed jet holes, with the aim of enhancing turbulent mixing and further diluting the main premixed flame.

## METHODOLOGY

Favre-Averaged Navier-Stokes (FANS) simulations have been performed on the Turbec T100 combustor. Due to the particular combustion regime inside the combustor, we have analyzed different combustion models, spanning from reaction-rate to primitive variable methods. More specifically we compare species transport, non-premixed and partially premixed modelling approaches, employing a reduced kinetic mechanism. The commercial code Fluent 19.2 by ANSYS Inc., based on the finite volume method, is used for all the simulations. Data provided by the manufacturer for the outlet concentration of CO and $NO_x$ are used to identify the best model. In the following sections we show the model equations solved by the code.

## Physical model

FANS equations for continuity, momentum and energy are solved in steady-state conditions:

$$\nabla \cdot (\bar{\rho}\tilde{\boldsymbol{u}}) = 0 \tag{1}$$

$$\nabla \cdot (\bar{\rho}\tilde{\boldsymbol{u}}\tilde{\boldsymbol{u}}) = -\nabla \bar{p} + \nabla \cdot \bar{\boldsymbol{T}} - \nabla \cdot \left(\bar{\rho}\widetilde{\boldsymbol{u}''\boldsymbol{u}''}\right) \tag{2}$$

$$\nabla \cdot \left(\bar{\rho}\tilde{h}\tilde{\boldsymbol{u}}\right) = \nabla \cdot \left(\overline{\rho\alpha\nabla h}\right) - \nabla \cdot \left(\bar{\rho}\widetilde{h''\boldsymbol{u}''}\right) - \overline{\sum_{1}^{N} h_k \dot{\omega}_k} + Q_{rad} \tag{3}$$

where a generic variable $\phi$ can be written as $\phi = \tilde{\phi} + \phi''$, in which $\tilde{\phi} = \overline{\rho\phi}/\bar{\rho}$ is the Favre average of $\phi$. In the above set of equations **u** is the velocity, $p$ is the pressure, **T** is the stress tensor, and $h$ is the enthalpy; $\rho$ and $\alpha$ represent the density and the thermal conductivity, respectively. Some terms in equations (1-3) need to be closed. Due to the presence of swirls, separations, and recirculation zones in the flow, the Realizable $k$-$\varepsilon$ model is employed for the closure of the Reynolds Stress Tensor, i.e. $\bar{\rho}\widetilde{\boldsymbol{u}''\boldsymbol{u}''}$. The turbulent transport of heat, i.e., $\bar{\rho}\widetilde{h''\boldsymbol{u}''}$, is modelled by applying the gradient transport hypothesis, with a turbulent Prandtl number of $Pr_t$ = 0.85 (Vodret et al., 2014). Radiation is taken into account with the Discrete-Ordinates model by solving 2x2 directions for each octant and by using the Weighted-Sum of Gray Gases (WSGG) model for the radiation properties of the gas, with coefficients by Smith et al., 1982. For what concern the combustion model, we have employed different approaches, based on different considerations, as shown in the following sub-sections. KEE58 scheme with 17 chemical species and 58 reversible reactions (Bilger et al., 1990) is employed as a reaction mechanism in all simulations. This mechanism has been largely applied for modeling $H_2$-enriched methane flames (e.g., Aminian et al. 2012) showing a good compromise between accuracy and computational cost. NOx formation is modelled taking into account Thermal, Prompt and $N_2O$-intermediate paths; in particular, Thermal NOx rate coefficients are based on the evaluation of Hanson and Salimian, 1984, using instantaneous concentration of O and OH radicals; Prompt NOx formation is evaluated using a global kinetic parameter derived by De Soete, 1975; $N_2O$-intermediate mechanism is taken into account using kinetic rate constants proposed by Malte and Pratt, 1972. In addition, when hydrogen is added to the fuel mixture, also the NNH mechanism (Konnov et al., 2000) is considered, since it can play a role in $NO_x$ formation. Instantaneous re-burning of NOx is also taken into account, with reaction rates coefficients from Bowman, 1991. Methane/hydrogen admixtures have been analysed in this work, considering two main cases based on the hydrogen contribution to the total thermal power and indicated as 0%$H_2$ and 25%$H_2$ (Table 1). 25%$H_2$ corresponds to a hydrogen mass fraction of about 12% in the fuel mixture, and at this concentration flashback occurs, as reported in LES simulations by Pappa et al. (2021). All the cases have been simulated for a total thermal output of 345 $kW_{th}$. The absolute operating pressure is set to 4.5 bar.

**Table 1: Thermal power contribution of $CH_4$ and $H_2$ for *0%$H_2$* and *25%$H_2$* cases.**

| Case | 0%$H_2$ | 25%$H_2$ |
|---|---|---|
| Thermal input $CH_4$ [$kW_{th}$] | 345 | 258.75 |
| Thermal input $H_2$ [$kW_{th}$] | 0 | 86.25 |

## Combustion models

### *Non-premixed model – Steady Laminar Flamelets (SLF)*

As fuel and air enter the domain in distinct streams, a non-premixed model is adopted. The non-premixed combustion model is based on the assumption that the thermo-chemical state of the system can be reduced to a single conserved scalar quantity, called mixture fraction, $Z$. A transport equation for $Z$ can be written as follows:

$$\nabla \cdot \left(\bar{\rho}\tilde{\boldsymbol{u}}\tilde{Z}\right) = \nabla \cdot \left(\overline{\rho D \nabla Z}\right) - \nabla \cdot \left(\bar{\rho}\widetilde{\boldsymbol{u}''Z''}\right) \tag{4}$$

where $D$ is the mass diffusivity. Being $Z$ a conserved scalar, no source terms appear in equation 4, so combustion is reduced to a mixing problem. Chemistry is modelled through a Steady Laminar Flamelet approach. This approach considers the structure of turbulent flames as an ensemble of laminar flames, or flamelets, which are able to describe the flame front locally (Peters, 1984). Data on flamelets for non-premixed combustion are derived from experiments or calculations, feeding fuel and oxidizer in an opposed axisymmetric configuration at different strain values (Dixon-Lewis, 1990). Then, turbulence-chemistry interaction is taken into account by generating assumed-shape Probability Density Function (PDF), so as to relate the local flamelet description to the turbulent flame front. Detailed kinetic mechanisms can be included in this approach. Species concentrations are derived from the predicted mixture fraction field, avoiding solving transport equations for individual species, thus saving CPU time.

*Partially premixed model – Flamelet Generated Manifold (FGM)*

Even if fuel and air enter the computational domain in separated streams, a strong mixing occurs before combustion takes place, producing a quite homogeneous fuel/air mixture entering the combustion chamber. To this purpose, a partially premixed model could be a reasonable choice to describe the combustion regime for the case under investigation. The partially premixed model exhibits properties of both non-premixed and premixed models. In the premixed combustion model, the reacting mixture is divided into two regions: unburned reactants and burned combustion products, separated by the flame sheet. To describe these two regions a progress variable C is introduced, assuming values from 0 to 1, (0 unburned mixture, 1 burned mixture). A transport equation for C can be written as follows:

$$\nabla \cdot \left(\bar{\rho}\widetilde{\boldsymbol{u}}\widetilde{\mathrm{C}}\right) = \nabla \cdot \left(\overline{\rho D \nabla C}\right) - \nabla \cdot \left(\bar{\rho}\widetilde{\boldsymbol{u}''C''}\right) + \bar{\dot{\omega}} \tag{5}$$

where $\bar{\dot{\omega}}$ is the reaction rate of progress variable C. As for non-premixed combustion, also premixed combustion is modelled through a flamelet approach. Data on premixed flamelets are obtained from experiments or simulations, consisting in a single jet in which the air/fuel mixture is perfectly mixed. Van Oijen, 2002, demonstrated through numerical simulations that partially premixed combustion can be appropriately modelled using chemical dataset of premixed flamelets, when the length scale associated to the mixture fraction gradient (∇Z) is much larger than the flame thickness $\delta_L$:

$$(\nabla Z \cdot \nabla Z)^{-0.5} \gg \delta_L \tag{6}$$

Due to the very fast mixing between air and fuel, condition (6) is fully verified, except for some little regions near the fuel inlets (De Santis, 2016). Hence, for the case under investigation, premixed combustion prevails over non-premixed combustion, implying that using a premixed flamelets database can better predict the combustion regime. The premixed flamelet library is generated using the Flamelet Generated Manifold method (Van Oijen, 2000), considering non-adiabatic conditions, with the possibility of implementing detailed kinetic mechanisms. Turbulence-chemistry interactions are taken into account by using a joint-PDF for the progress variable C and the mixture fraction Z.

*Species transport - Eddy Dissipation Concept (EDC)*

Species concentration field can be derived by solving a transport equation for each species, as follows:

$$\nabla \cdot \left(\bar{\rho}\tilde{Y}_k\widetilde{\boldsymbol{u}}\right) = \nabla \cdot \left(\overline{\rho D_k \nabla Y_k}\right) - \nabla \cdot \left(\bar{\rho}\widetilde{Y_k''\boldsymbol{u}''}\right) + \overline{\dot{\omega}_k} \tag{7}$$

where $Y_k$, $D_k$ and $\overline{\dot{\omega}_k}$ are the mass fraction, the mass diffusivity, and the average production/consumption of the *k*-th species due to chemical reactions, respectively. Closure of $\overline{\dot{\omega}_k}$ is achieved through the Eddy Dissipation Concept (EDC) combustion model. The EDC model assumes that combustion takes place in fine structures where the turbulence kinetic energy associated to the flow is dissipated. In the original model (Magnussen 1981; Magnussen, 2005), the fine structures are modelled as Perfectly Stirred Reactors (PSR), however Ansys Fluent considers them as Plug Flow Reactors (PFR) as it can improve the robustness, with negligible differences in results (Li et al, 2017)

## Numerical settings

The computational domain is fully derived from the combustion chamber of the micro-Gas Turbine Turbec T100, simplifying only few geometrical details. A grid sensitivity analysis was carried out to optimise the number of cells, generating six meshes from 542k to 2.60M cells with a refinement ratio of about 1.37. The chosen grid consists of 1.7M cells, with polyhedrons in the internal volume and prism layers at the walls (Figure 2). Particular attention was paid in ensuring a higher cells density inside the combustion chamber than in the external case.

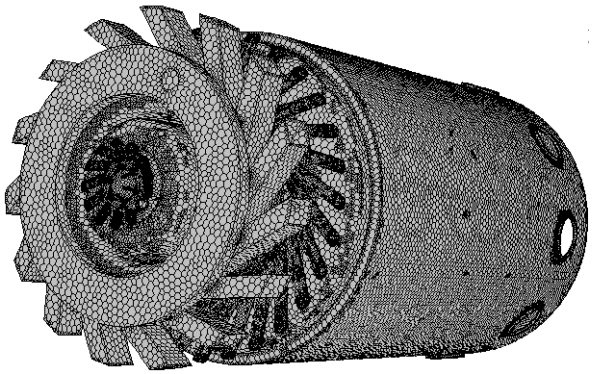

**Figure 2: Computational grid.**

As for the wall functions, the enhanced wall treatment was employed with a mean value of 36 for $y^+$. Boundary conditions consist of: mass flow inlet, temperature and composition at the air and fuel inlets (see Table 2); pressure outlet with average pressure specification at the exit; no slip condition and zero heat flux (adiabatic operation) at the walls. Conjugate heat

transfer calculations were not carried out, to reduce the calculation time. A second order upwind interpolation scheme was employed with the semi-implicit Coupled algorithm. At convergence normalized residuals did not change with iterations and were all well below $10^{-4}$. Only continuity residual stabilized at $10^{-3}$, because of the complexity of the flow field. Besides, physical variables were monitored to confirm convergence. For the sake of completeness, Table 3 summarises the simulations performed in this work.

**Table 2: Boundary conditions.**

| **Case A: 0%$H_2$** | | | |
|---|---|---|---|
| Boundaries | Air inlet | Main fuel inlet | Pilot fuel inlet |
| Mass flow·$10^3$ [kg/s] | 777.6 | 5.886 | 1.014 |
| Temperature [K] | 868 | 298 | 298 |
| $CH_4$ mass fraction [-] | 0 | 1 | 1 |
| $H_2$ mass fraction [-] | 0 | 0 | 0 |
| $O_2$ mass fraction [-] | 0.23 | 0 | 0 |
| **Case B: 25%$H_2$** | | | |
| Mass flow·$10^3$ [kg/s] | 777.6 | 5.304 | 0.589 |
| Temperature [K] | 868 | 298 | 298 |
| $CH_4$ mass fraction [-] | 0 | 0.878 | 0.878 |
| $H_2$ mass fraction [-] | 0 | 0.122 | 0.122 |
| $O_2$ mass fraction [-] | 0.23 | 0 | 0 |

**Table 3: List of simulations.**

| Simulations | $H_2$ thermal input [%] | Combustion model |
|---|---|---|
| 0%$H_2$_EDC | 0 | EDC |
| 0%$H_2$_FGM | 0 | FGM |
| 0%$H_2$_SLF | 0 | SLF |
| 25%$H_2$_EDC | 25 | EDC |
| 25%$H_2$_FGM | 25 | FGM |

## RESULTS AND DISCUSSION

### *Case A: 0%$H_2$*

Preliminary, 3-dimensional steady-state CFD simulations were performed for the Turbec T100 combustor fed with natural gas. The velocity magnitude field on the combustor mid-plane is shown in Figure 3 for the simulation with EDC (i.e., 0%$H_2$_EDC), but similar considerations can be made for the others. Figure 3 shows that a large flow rate of air passes through the dilution holes, acting as a barrier for the gases coming from the upstream regions. This flow configuration produces two recirculation zones inside the combustion chamber: an inner recirculation zone (IRZ) and an outer recirculation zone (ORZ). In between these two low velocity regions, there is a high velocity jet (about 100 m/s) generated by the rapid expansion of the combustion gases from the main premixed flame. The flow field in the pilot region is quite similar, with a high velocity jet confined between two small recirculation zones.

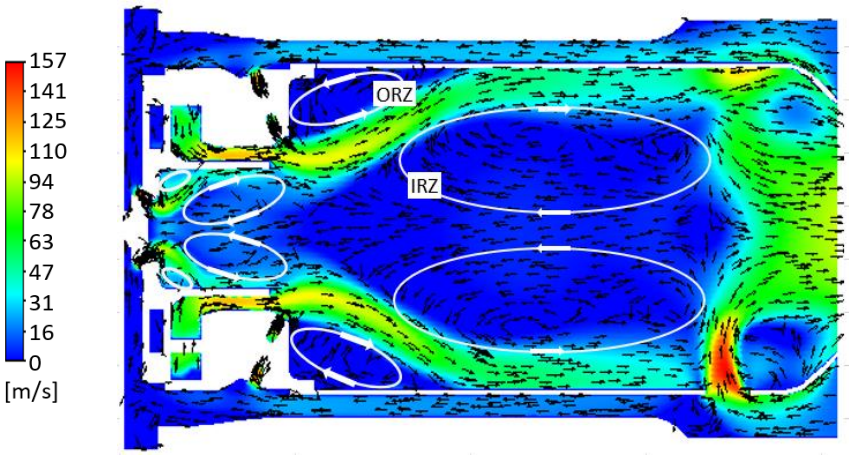

**Figure 3: Velocity magnitude field predicted by the 0%$H_2$_EDC simulation.**

Pressure drops calculated by the models are summarized in Table 4, compared to the value provided by the manufacturer. All the models slightly underpredict the total pressure drops, however the agreement with the experimental value can be considered satisfying.

**Table 4: Predicted and experimental total pressure drops.**

| Models | EDC | FGM | SLF | EXP |
|---|---|---|---|---|
| Total pressure drop [Pa] | 24509 | 24037 | 26068 | 26760 |

Figure 4 shows the temperature field inside the combustor when different combustion models are employed. Figures 4.a and 4.b are quite similar except for few details. In fact, the Flamelet Generated Manifold shows higher temperature, with the main flame more developed in the axial direction. In addition, the FGM model predict higher temperatures near the outer recirculation zone (ORZ) with respect to the temperatures predicted by the EDC. Some differences can also be noticed in the pilot region, with a faster ignition of the pilot flame predicted by the FGM model. The temperature field depicted in Figure 4.c is different from the others, showing higher temperatures and a flashback in the premixing duct of the main flame. However, the flashback does not occur during the actual operation of the combustor, when fuelled with pure methane. For this reason, the non-premixed flamelets model cannot capture the combustor behaviour.

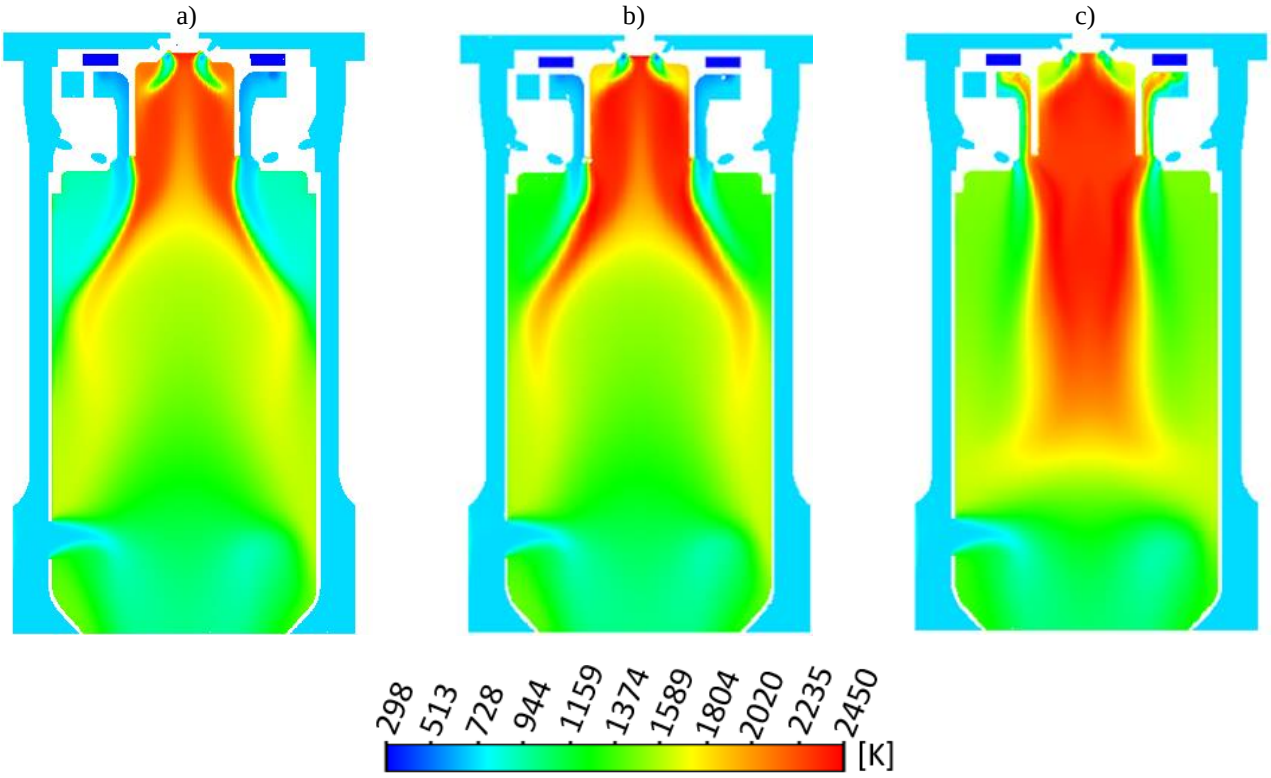


**Figure 4: Temperature field on the combustor mid-plane predicted by: a) EDC, b) FGM and c) SLF.**

Table 5 shows the predicted concentrations of carbon monoxide (CO) and nitrogen oxides ($NO_x$) at the exit of the combustor considering 15% of $O_2$ in the outlet stream. Experimental concentrations provided by the manufacturer are CO@15%$O_2$ < 15 ppm and $NO_x$@15%$O_2$ < 15 ppm.

**Table 5: Predicted and experimental CO and $NO_x$ concentrations. Case A: 0%$H_2$.**

| Models | EDC | FGM | SLF | EXP |
|---|---|---|---|---|
| CO@15%$O_2$ [ppm] | 683 | 0.3 | 9 | < 15 |
| $NO_x$@15%$O_2$ [ppm] | 61 | 80 | 104 | < 15 |

CO concentration in the exhaust gases is well predicted by FGM and SLF models, showing a complete combustion of the fuel as declared by the manufacturer. Instead, the EDC model highly overpredicts CO in the outlet stream. Indeed, for such model, Figure 4.a shows lower temperatures close to the outer recirculation zone (ORZ), as a result of the main flame extinction (Aminian, 2016). All the models overpredict $NO_x$ concentrations. This general trend might be slightly correlated to the absence of a conjugate heat transfer model, which would have reduced the maximum temperatures. The highest $NO_x$ value is obtained with the SLF model, as a consequence of the high temperatures predicted inside the combustion chamber. Thermal and $N_2O$-intermediate formation paths represent the main share of the total $NO_x$, contributing for 73.6% and 25.8% respectively, while the prompt contribution is negligible. Figure 5 shows the NO molar fraction distribution for the 0%$H_2$_EDC simulation, indicating that NO formation is mainly located near the non-premixed pilot flame.

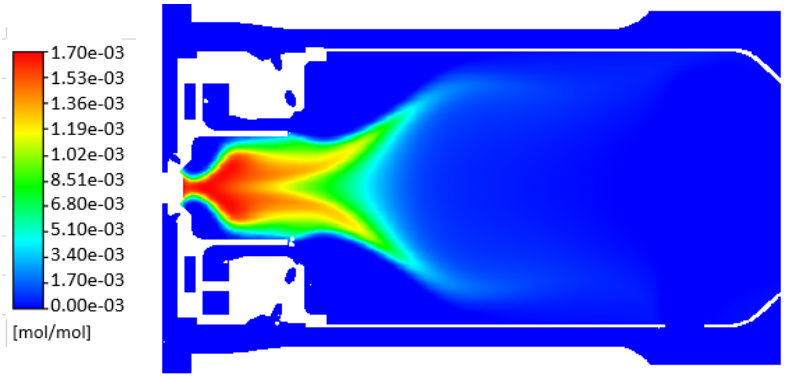


**Figure 5: NO molar fraction distribution inside the combustor.**

*Case B: 25%$H_2$*

Figure 6 shows the temperature field for the 25%$H_2$ case as predicted by: a) the EDC model and b) the FGM model. The temperatures reached in this case are about 50°C higher respect to the case with pure methane (0%$H_2$). This happens because hydrogen increase the adiabatic flame temperature and the reactivity of the fuel mixture. Even though the hydrogen content in the fuel mixture is low, LES simulations by Pappa et al., 2021 demonstrated that flashback occurs in the premixing vane of the main flame. This phenomenon is not predicted by the EDC model (Figure 6.a), while it is captured by the FGM model (Figure 6.b), showing a slight temperature increase inside the premixing vane.

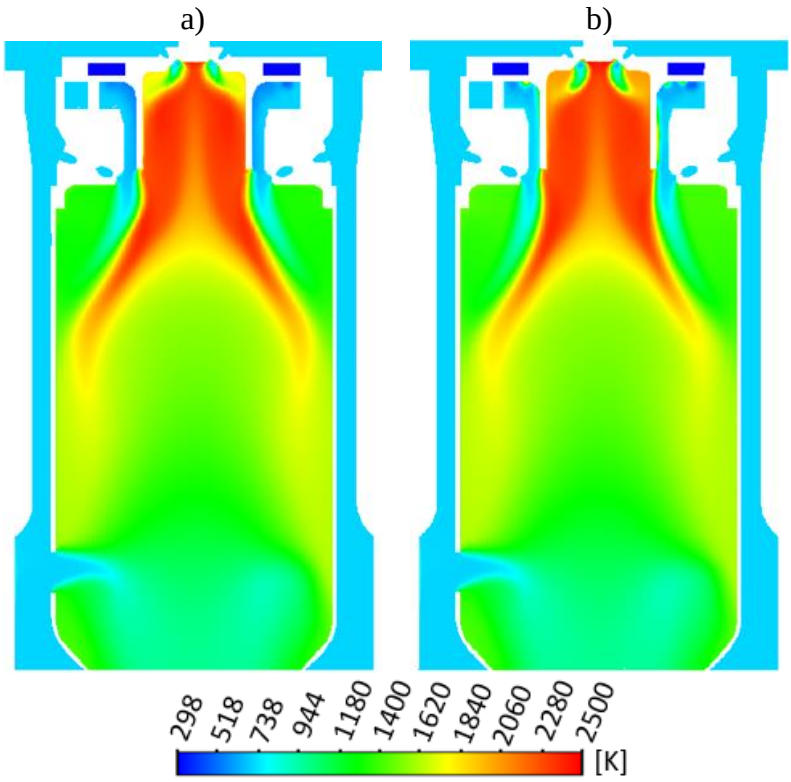

**Figure 6: Temperature field predicted by a) EDC and b) FGM.**

Comparing Figure 5.a with Figure 6.a, it is possible to observe that in the ORZ the temperature is higher when hydrogen is added to the fuel mixture, resulting in a more efficient combustion of the main premixed flame. This is confirmed by the values reported in Table 6 for CO and $NO_x$ concentrations in the outlet stream. The CO concentration provided by EDC reduces significantly compared to the methane case. Indeed, hydrogen enhances the fuel reactivity, increasing the reaction yield, hence CO consumption; hydrogen itself does not contain carbon atoms, reducing the production of carbon-based species. However, the CO concentration is still over-estimated, while FGM provides a value in line with the manufacturer's specifications.

**Table 6: CO and NOx concentrations predicted by the models. Case B: 25%$H_2$.**

| Models | EDC | FGM |
|---|---|---|
| CO@15%$O_2$ [ppm] | 288 | 0.2 |
| $NO_x$@15%$O_2$ [ppm] | 145 | 88 |

$NO_x$ concentrations predicted by the models increase, because of the higher temperatures reached in the combustion chamber, which enhance Thermal $NO_x$ formation (about 98.7% of the total). The NNH path does not play a key role (0.2%), as $H_2$ fraction in the fuel mixture is low.

## CONCLUSIONS

A commercial mGT combustor is analyzed through Computational Fluid-Dynamics techniques, assuming steady-state conditions. Due to the complex combustion regime, different combustion models are compared to capture the actual behavior of the combustor. The comparison shows that the FGM model provides the best results in terms of predicted temperature field and concentrations of CO and $NO_x$. The SLF model, which uses a library based on non-premixed flamelets, cannot describe accurately the temperature field inside the combustor, predicting a flashback even for the 0%$H_2$ case, that is not in agreement with experimental observations. On the other hand, the EDC model is able to describe the general functioning of the combustor, even though it predicts the extinction of the main premixed flame, resulting in a high over-prediction of the CO concentration in the outlet.

Results from the case 25%$H_2$ show that the combustor under investigation is able to work properly, when the fuel is enriched with a low mass fraction of hydrogen. However, a higher reactivity of the fuel mixture is noticed with the possibility of flashback issues. We believe that the present work provides a useful analysis of the available combustion modelling techniques and is able to describe the thermo-chemical behavior of a commercial mGT combustor.

## REFERENCES


Abagnale, C., Cameretti, M. C., De Robbio, R., Tuccillo, R. (2016). CFD Study of a MGT Combustor Supplied with Syngas. *Energy Procedia*, 101, pp. 933-940. https://doi.org/10.1016/j.egypro.2016.11.118.

Ali, U., Best, T., Finney, K., Font-Palma, C., Hughes, K., Ingham, D., Pourkashanian, M. (2014). Process Simulation and Thermodynamic Analysis of a Micro Turbine with Post-combustion CO2 Capture and Exhaust Gas Recirculation. *Energy Procedia*, 63, pp. 986-996. https://doi.org/10.1016/j.egypro.2014.11.107.

Aminian, J., Galletti, C., Shahhosseini, S., Tognotti, L. (2012). Numerical investigation of a MILD combustion burner: Analysis of mixing field, chemical kinetics and turbulence-chemistry interaction. *Flow, Turbulence and Combustion*, 88, pp. 597-623. https://doi.org/10.1007/s10494-012-9386-z.

Aminian, J., Galletti, C., Tognotti, L. (2016). Extended EDC local extinction model accounting finite-rate chemistry for MILD combustion. *Fuel*, 165, pp. 123-133. https://doi.org/10.1016/j.fuel.2015.10.041.

Bilger RW, Pope SB, Bray KNC, Driscoll JF (2005). Paradigms in turbulent combustion research. *Proc Combust Inst*, 30, pp. 21–42. https://doi.org/10.1016/j.proci.2004.08.273

Bowman, C.T. (1991). Chemistry of Gaseous Pollutant Formation and Destruction. *Fossil Fuel Combustion*.

Cameretti, M. C., Cappiello, A., De Robbio, R., Tuccillo R. (2020). Comparison between Hydrogen and Syngas Fuels in an Integrated Micro Gas Turbine/Solar Field with Storage. *Energies*, 13, pp. 47-64. https://doi.org/10.3390/en13184764

Cappelletti, A., Martelli, F., Bianchi, E., Trifoni, E. (2014). Numerical Redesign of 100kw MGT Combustor for 100% H2 fueling. *Energy Procedia*, 45, pp. 1412-1421. https://doi.org/10.1016/j.egypro.2014.01.148.

De Santis, A., Ingham, DB, Ma, L., Pourkashanian, M. (2016). CFD analysis of exhaust gas recirculation in a micro gas turbine combustor for CO2 capture. *Fuel*, 173, pp. 146-154. https://doi.org/10.1016/j.fuel.2016.01.063.

De Soete, G. (1975). Overall reaction rates of NO and N2 formation from fuel nitrogen. *Proceedings of the Symposium (International) on Combustion*, 15, pp. 1093–1102.

Dixon-Lewis, G. (1991). Structure of Laminar Flames. *Symposium (International) on Combustion*, 23, pp. 305-324. https://doi.org/10.1016/S0082-0784(06)80274-2.

Hanson, RK, and Salimian, S. (1984). Survey of Rate Constants in H/N/O Systems. *Combustion Chemistry*.

Konnov, A., Colson, G., De Ruyck, J. (2000). The new route forming NO via NNH. *Combust. Flame*, 121, 548–550.

Li, Z., Cuoci, A., Sadiki, A., Parente, A. (2017). Comprehensive numerical study of the Adelaide Jet in Hot-Coflow burner by means of RANS and detailed chemistry. *Energy*, 139, pp. 555-570. https://doi.org/10.1016/j.energy.2017.07.132.

Magnussen, B. F. (2005). The Eddy Dissipation Concept: a bridge between science and technology. In: *ECCOMAS Thematic Conference on Computational Combustion, Lisbon, Portugal*.

Magnussen, B. F. (1981). On the structure of turbulence and a generalized eddy dissipation concept for chemical reactions in turbulent flow. In: *19th AIAA, Sc. Meeting, St. Louis, USA*.

Malte, P., and Pratt, D. (1975). Measurement of Atomic Oxygen and Nitrogen Oxides in Jet Stirred Combustion. *Symposium (International) on Combustion*, pp 1061-1070. https://doi.org/10.1016/S0082-0784(75)80371-7.

Pappa, A., Bricteux, L., Bénard, P., De Paepe, W. (2021). Can Water Dilution Avoid Flashback on a Hydrogen-Enriched Micro-Gas Turbine Combustion? - A Large Eddy Simulations Study. *Journal of Engineering for Gas Turbines and Power,* 143. DOI: 10.1115/1.4049798.

Peters., N. (1984). Laminar Diffusion Flamelet Models in Non Premixed Combustion. *Prog. Energy Combust. Sci*., 10, pp. 319-339.

Reale, F., Calabria, R., Chiariello, F., Pagliara, R., and Massoli, P. (2012). A Micro Gas Turbine Fuelled by Methane-Hydrogen Blends. *Applied Mechanics and Materials*, 232, pp. 792–796.

Shih, H.-Y., and Liu, C.-R. (2014). A computational study on the combustion of hydrogen/methane blended fuels for a micro gas turbines. *International Journal of Hydrogen Energy*, 39, pp. 15103-15115. https://doi.org/10.1016/j.ijhydene.2014.07.046.

Smith, T. F., Shen, Z. F., and Friedman, J. N. (1982). Evaluation of Coefficients for the Weighted Sum of Gray Gases Model. *ASME. J. Heat Transfer*, 104, pp. 602–608. https://doi.org/10.1115/1.3245174

Tomczak, H., Benelli, G., Carrai, L. (2002). Investigation of a gas turbine combustion system fired with mixtures of natural gas and hydrogen. *IFRF Combustion Journal*, 19, pp. 200-207.

van Oijen JA., and de Goey LPH. (2000). Modelling of premixed laminar flames using flamelet-generated manifolds. *Combustion Science and Technology*, 161, pp.113-137. https://doi.org/10.1080/00102200008935814.

van Oijen JA. (2002). Flamelet generated manifolds: development and application to premixed laminar flames. PhD thesis. Eindhoven University of Technology.

Vodret, S., Di Maio, V., Caruso, G. (2014). Numerical simulation of turbulent forced convection in liquid metals. *Journal of Physics: Conference Series*, 547, pp. 12-33.